Paper pa17-026
Submitted to the 28th International Conference on High Energy Physics
ICHEP'96, Warsaw, Poland, July 1996

Luminosity Measurement in the H1 Experiment at HERA

H1 Collaboration

Abstract

The methods used to obtain precision measurements of both the instantaneous and the integrated luminosities in the H1 detector, operating at the electron-proton collider HERA, are presented. The H1 luminosity monitor consists of two crystal calorimeters which are placed at distances of 33 m and 103 m from the ep interaction point. The Bethe-Heitler reaction $ep \rightarrow e\gamma p$ is used to determine the luminosity. Both the photon and the scattered electron are detected , meaning that different methods of luminosity measurement are possible. In this way systematic uncertainties can be controlled with high precision. The system is free of dead time and can operate safely in a hostile radiation environment. During ep collision data taking, the system provides permanent monitoring of the electron beam parameters and of the relative luminosity with a statistical precision of 2%/s, permitting it to be used for accurate tuning of beam optics and for fast optimisation of the specific luminosity in the H1 interaction region. The sources of systematic errors in the determination of the absolute integrated luminosity are presented. A precision of $\pm 1.1\%$ is achieved for the data accumulated in 1995.

1 Introduction

The method of luminosity measurement at HERA, used by the H1 and ZEUS experiments, is based on the Bethe-Heitler (BH) reaction

$$ep \rightarrow e\gamma p. \tag{1}$$

The instantaneous (L) and integrated ($\mathcal{L}$) luminosities are then calculated as

$$L = \frac{R_{BH}}{\sigma_{BH}}; \qquad \mathcal{L} = \frac{N_{BH}}{\sigma_{BH}}, \tag{2}$$

where R, N and σ denote the rate, the number of events and the cross section [1] of reaction (1) respectively. There are however several technically different methods to identify the reaction (1) and to calculate R (or N) in (2). Of these the following are used:

- the *coincidence* method requires the simultaneous detection of e and γ in the final state,
- the *single photon* method counts the rate (the number of events) in (2) with the photon energy above a certain threshold.

The discussion on the advantages and drawbacks of these methods can be found in [2, 3]. For the online luminosity measurement by the H1 Luminosity Monitor the *coincidence* method is applied. For the offline determination of the final value of the integrated luminosity $\mathcal{L}$, the *single photon* method is used. Both measurements are presented here. In 1995 HERA collided e^+- and p- beams of 27.5 GeV and 820 GeV respectively.

The paper is organized as follows: in section 2 a general description of the H1 Luminosity System is given. Section 3 describes the data sample for the 1995 analysis. The details of the procedure to determine the integrated luminosity with the *single photon* method, together with the results obtained, are described in section 4.

2 The Luminosity System

The luminosity system serves several purposes. Its main task is a fast relative luminosity measurement with a statistical precision of $\sim 2\%$ at nominal beam conditions. It also provides electron beam monitoring for the HERA machine, absolute online luminosity measurement with an accuracy of $\sim 5\%$, energy measurement for electrons scattered under small angles (tagging of photoproduction events) and measurement of photons from initial state radiation.

2.1 System Overview

The luminosity is determined from the rate of Bethe-Heitler events $ep \rightarrow ep\gamma$. The main source of background is bremsstrahlung from the residual gas in the beam pipe, $eA \rightarrow eA\gamma$. At design luminosity (L $= 1.5 \times 10^{31}$ cm^{-2}s^{-1}) these events are expected at 10 % of the $ep \rightarrow ep\gamma$ rate, but can be subtracted using data from electron pilot bunches (e-bunches without colliding p-bunches). The luminosity is calculated as

$$L = \frac{R_{tot} - (I_{tot}/I_0)R_0}{\sigma_{vis}},$$

where R_{tot} is the total rate of the bremsstrahlung events, R_0 is the rate for electron pilot bunches, I_{tot} and I_0 are the corresponding electron beam currents and σ_{vis} is the visible part of the Bethe-Heitler cross-section with acceptance and trigger efficiency included.

The luminosity monitor detects scattered electrons and outgoing photons in coincidence. It consists of two arms: the electron tagger (ET) and the photon detector (PD). Since the angular distributions for both the electrons and photons are strongly peaked in the direction of the primary e-beam – polar angles are of the order of $\theta \simeq O(m/E) \simeq$ 17 μrad at 30 GeV – the detectors have to be placed close to the beampipe and far from the interaction region in order to cover these small angles.

The general view of the luminosity system is shown in Fig.1. Scattered electrons are deflected by a set of low-beta quadrupoles and a bending magnet located in the region 5.8 m $< -z <$ 23.8 m, pass an exit window at $-z =$ 27.3 m and hit the ET at $-z =$ 33.4 m. The photons leave the proton beampipe through a window at $-z =$ 92.3 m, where the beam pipe bends upward, and hit the PD at $-z =$ 102.9 m. A Pb filter (2.2 X_0) followed by a water Čerenkov (0.8 X_0) veto counter (VC) protects the detector from the high synchrotron radiation flux. From the p-beam side the PD is shielded by an iron wall of 2 m thickness. The VC eliminates events with photons interacting in the filter. The ET and the PD together with VC can be remotely moved out of the median plane of the e-beam during injection. This operation can be reversed within $1 - 2$ minutes with a position accuracy of $\sim$ 100 μm.

The acceptance of the luminosity system for nominal electron beam conditions ($E_e =$ 27.5 GeV, zero tilt) and the expected rates at the design luminosity of 1.5×10^{31} cm^{-2}s^{-1} are given in Table 1. One of the main contributions to the systematic error in the luminosity measurement comes from the dependence of the system acceptance on possible variations of the electron beam angle in the interaction region. This tilt, typically of the order of 100 μrad, is controlled by the position of the photon-beam profile at the PD with high precision, of the order of 10 μrad. The corresponding corrections to σ_{vis} are taken into account already online and can be further improved during the offline analysis. Quasi-real photoproduction events with $Q^2 < 0.01$ GeV^2 can be tagged by the ET in the energy interval $0.2 < E_{e'}/E_e < 0.8$ using both PD and VC signals as a veto.

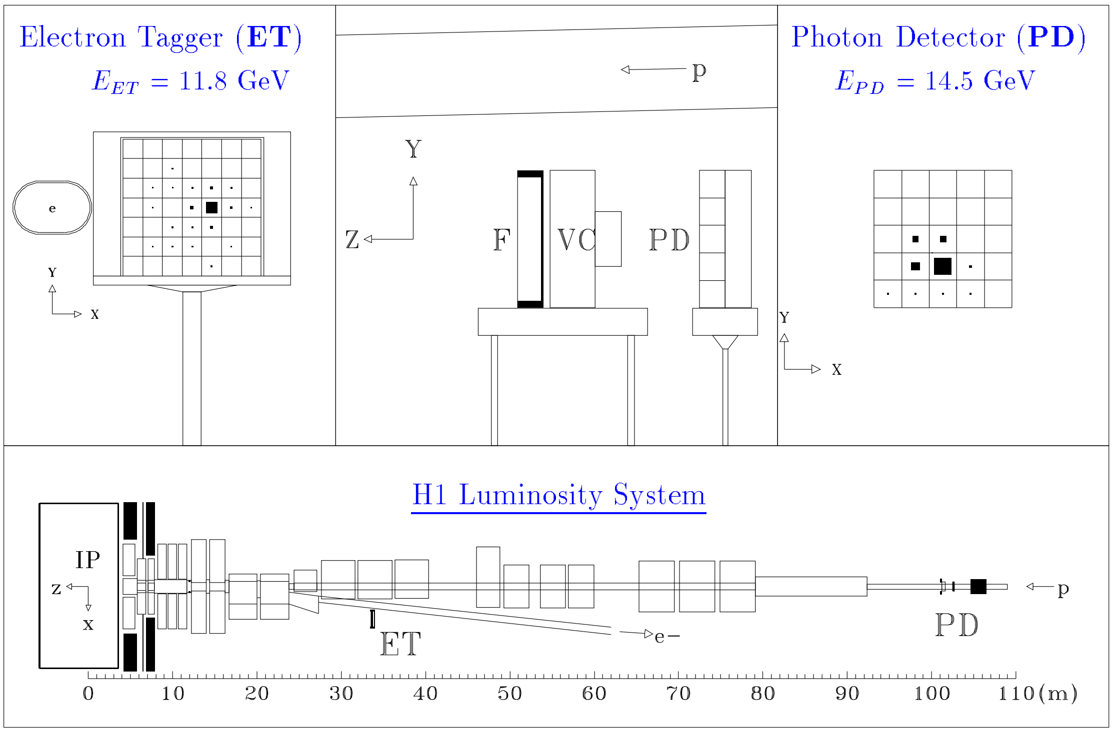

Figure 1: The layout of the luminosity system.

	unit	ET	PD
Energy interval, $E_\gamma/E_e = 1 - E_{e'}/E_e$		$0.2 - 0.8$	$0.004 - 1.0$
Polar angle acceptance interval	mrad	$0 - 5$	$0 - 0.45$
Average acceptance for $ep \to ep\gamma$	%	48	98
Average acceptance for photoproduction	%	36	−
σ_{vis}	mb	28	174
$ep \to ep\gamma$ rate for $E > E_{thr} = 4$ GeV [1]	MHz	0.4	1.3
Photoproduction event rate [1]	Hz	$20 - 30$	−
Aperture $x \times y$ (granularity)	mm^2	154×154 (7×7)	100×100 (5×5)
Chemical composition		TlCl(78%) + TlBr(22%)	
Radiation length (Molière radius)	cm	0.93 (2.10)	
Crystal length (radiation hardness)	cm (Rad)	20 $(> 6 \cdot 10^7)$	
Energy resolution, σ_E/E [2]	%	$1 \oplus 10/\sqrt{E}$, (E in GeV)	
Position (time) resolution, $\sigma_{x,y}$ (σ_t) [2]	mm (ns)	$0.3 - 1.2$ (< 3)	

Table 1: Parameters of the luminosity system. [1] at design luminosity; [2] values reached at HERA.

2.2 Detectors

The design goals – high radiation resistance, good energy, coordinate and time resolution and compactness – were best met by a hodoscope of total absorption KRS-15 crystal Čerenkov counters. Their properties are summarized in Table 1.

Each calorimeter cell is viewed by a FEU-147 photomultiplier [4] with a 20 mm diameter cathode coupled to the crystal with an optical contact. The veto counter is viewed by two phototubes operating in different regimes, the first for photon detection, the second operating with increased voltage and reaching full efficiency for charged particles with a range exceeding 35 cm. Taking into account the material in front of the VC, this corresponds to full efficiency for electromagnetic showers initiated by the photons with $E_\gamma > 1.5$ GeV.

Since the luminosity detectors operate at high rates up to few MHz, which may vary within one beam filling by a factor of 3 to 10, they are permanently calibrated during data taking using the energy constraint $E_{ET} + E_{PD} = E_{e^+beam}$. Although the calibration coefficients may change within $5 - 20\%$, this method allows an absolute calibration with a precision of better than 1%.

The different functions of the luminosity system required a special trigger and data acquisition concept, based on the two completely independent branches. The photomultiplier signals pass first differential preamplifiers close to the detectors and then, after 170 m or 100 m of fast coaxial cable pairs, respectively, are again shaped and amplified at the trigger electronics crate. This solution reduces noise and compensates for signal attenuation in the cables. Then the signals are split and analysed in two groups of FADC's (2×80 channels).

The first FADC group operates in a standard mode, similar to all other subdetector trigger systems in H1. The trigger electronics discriminates the analog energy sums against the individually set thresholds, producing a dead time free trigger signal synchronized to the HERA beam crossing. Three basic trigger signals are available from the electron arm ($E_{ET} > E_{ET}^{thr}$), the photon arm ($E_{PD+VC} > E_{PD+VC}^{thr}$), and the veto counter. The front end readout and the data transfer to the central data acquisition are done by programs running on the FIC8230 master and slave processors [5].

The second FADC group is controlled locally and completely decoupled from the H1 trigger system. Several triggers are used for the luminosity calculation (ET$*$PD) and online detector calibration (ET$*$PD$*\overline{\text{VC}}$, ET$*$PD$*$VC). Any combination of 5 triggers can be permanently stored without dead time for each of the 220 bunches in a fast histogramming memory of 32×220 channels. This memory contains the full information on all bunch related trigger statistics, e.g. the level of accidental coincidences. The online event processing includes fast reconstruction, calibration, trigger verification and calculation of the current luminosity and is performed on a third FIC8230 processor.

The system has been working successfully since April 1992. A typical example of the information provided by the H1 Luminosity system during ep collisions is shown in Fig.2.

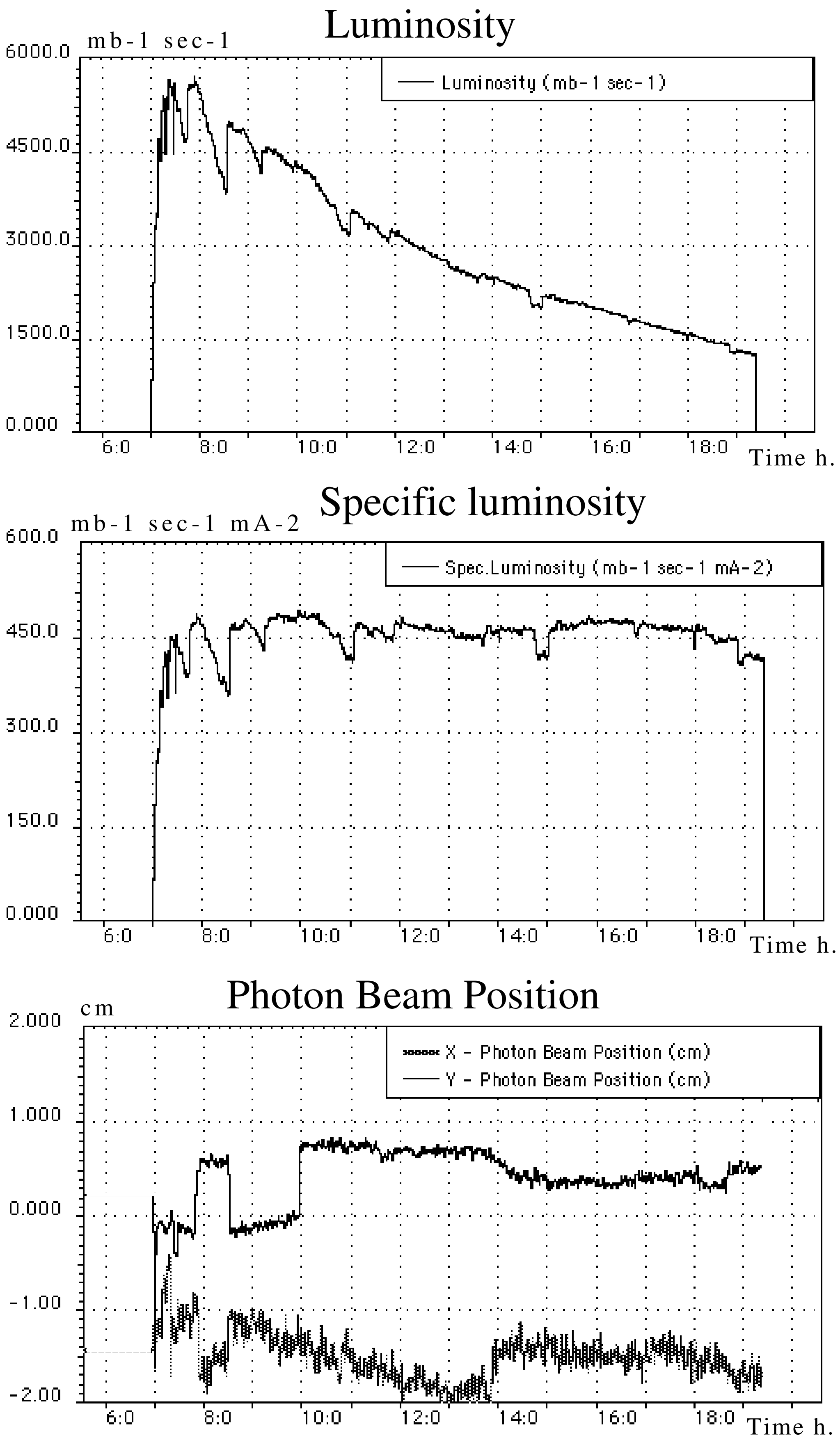

Figure 2: Data provided by the luminosity system during ep collisions at HERA. Statistical fluctuations correspond to one measurement every 10 s.

3 Data Sample

In order to carry out the offline monitoring and calibration of the H1 Luminosity system, as well as calculating offline integrated luminosity, a number of monitoring subtriggers (i.e. combinations of trigger signals) were introduced. They are described in Table 2. Several thresholds were used in the trigger signals composing these subtriggers. For the photon detector the thresholds were $PD_{low} \simeq 5.6$ GeV, $PD \simeq 6.2$ GeV and $PD_{high} \simeq 16.7$ GeV, for the electron tagger $ET \simeq 7.2$ GeV and for the veto counter $VC \simeq 0.5$ GeV. The total rate of these subtriggers was kept at about 1.0 Hz (using prescaling with factors 10^5 - 10^6).

Trigger	Purpose
s91 $= PD_{low}$	offline $\mathcal{L}$ determination
s92 $=$ PD$*\overline{\mathrm{VC}}$	calibration of ET and PD
s93 $=$ VC	VC calibration, tagging acceptance
s94 $=$ ET$*$PD$*\overline{\mathrm{VC}}$	calibration of ET and PD
s95 $=$ ET$*$PD$*$VC	calibration of ET, PD and VC

Table 2: Luminosity monitoring triggers used in 1995.

Events from these subtriggers are written to special summary tapes during data taking for convenient access in the offline analysis. In addition these tapes contain events triggered at random; they are used for trigger efficiency determination. For the offline determination of the integrated luminosity events triggered with **s91** were used.

The **s91** event-sample corresponding to the ep physics in 1995 constitutes about one million events. A summary of the luminosity accumulated in 1995 is given in Table 3.

Integrated luminosity	[nb^{-1}]
HERA produced (at final beam energies)	11055
HERA delivered to H1 (lumi declared)	10094
H1 gated (written on tapes)	6196
with H1 magnetic field on	5854
physics runs in the present analysis	5132

Table 3: The integrated luminosity in the H1 interaction region, as measured by the online Luminosity Monitor in 1995.

The data have been split into three different samples according to the position of the interaction point (IP) along the z axis. Some general characteristics of these data samples are summarized in Table 4. For comparison, the parameters of the 1994 nominal IP e^+p sample are also listed there.

Parameter	Unit	1995			1994
		nominal IP	z_{IP}=+70cm	z_{IP}=−70cm	e^+p
Number of physics runs		2890	114	59	1521
<Run time>	[s]	960	976	982	1803
<dead time>	[%]	17.7	10.6	17.1	13.0
Online $\mathcal{L}$	[nb^{-1}]	4936.6	145.7	49.5	3003.0
$< I_e >$	[mA]	18.7	18.0	17.9	17.1
$< I_p >$	[mA]	55.9	57.4	49.8	41.0
$< L >$	[μb^{-1}s^{-1}]	2.245	1.455	1.145	1.290
$< L_{sp} >$	[μb^{-1}s^{-1}mA^{-2}]	0.408	0.270	0.240	0.334
Bunches	$(ep + e + p)$	174 + 15 + 6			153+15+17

Table 4: Characteristics of three different data samples collected in 1995 by the H1 experiment. For comparison, the parameters of the 1994 e^+p nominal IP data are also listed.

4 Offline Luminosity Determination

As already mentioned in the introduction, the *single photon* method is used offline for the determination of the final value of the integrated luminosity.

Equations (2) look quite simple. Complications come when one tries to relate the number of observed events to the true number of events predicted by theory, and to calculate the acceptance corrected cross section σ_{BH}. Then in practice the integrated luminosity for the given data sample can be determined as

$$\mathcal{L} = \frac{N^{ep}_{BH}(E_\gamma > E_{min})}{\sigma_{BH}(E_\gamma > E_{min})} = \frac{\frac{\sum_i (W_i^{tot}(E_{min}) - W_i^{bgr}(E_{min}))}{\epsilon_{trig}(E_{min})}(1 - \delta_{n\gamma}(L, E_{min}))}{\sigma_{BH}(E_{min}) \cdot A_\gamma(\theta_x, \theta_y)}, \qquad (3)$$

where $W_i = P_i N_i$ represent the total and the background number of events in run i from the sample, after accounting for the (run dependent) prescaling P_i. E_{min} is the cutoff used in the analysis for the photon energy E_γ in PD. For simplicity only the most important parameters in equation (3) are listed in various functional dependencies. The geometrical acceptance A_γ is especially sensitive to the lepton beam tilt θ_x, θ_y in the interaction point. The pile-up effect (the probability to detect more than just one photon in the same bunch crossing) leads to a luminosity dependent correction $\delta_{n\gamma}(L, E_{min})$ in the number of observed events having an energy deposit above the cutoff E_{min}.

The choice of E_{min} usually represents a compromise between several partially conflicting demands, and must be optimized to reduce the final systematic error $\delta\mathcal{L}$.

The integrated luminosity has been determined in 1995 for three basic data samples, introduced in the previous section (see Table 4). They were further subdivided into smaller sub-samples characterized by significant changes observed in any of the critical parameters, such as the horizontal offset of the beam trajectory in the IP w.r.t. the H1 axis (as measured by the Central Tracking Chambers), the online luminosity system set up (high voltage settings, timing), accidents with the positron beam losses, which could influence the behavior of the luminosity detectors and the background conditions, etc. In total 19 different run periods have been defined and analyzed.

In order to achieve high precision in the determination of $\mathcal{L}$ through eq.(3), one has to understand in great detail:

- the measured E_γ spectrum, especially the absolute energy scale around E_{min},
- the background from e^+gas bremsstrahlung,
- **s91** trigger efficiency ϵ_{s91},
- the geometrical acceptance of the photon arm A_γ,
- the pile-up effect.

4.1 Choice of E_{min}

The energy distributions in the luminosity detectors are shown in Fig.3. The large tail at $E_\gamma > 30$ GeV is due to the pile-up effect. The energy resolution of the crystal calorimeters ET and PD corresponds in 1995 to $\sim 15\%/\sqrt{E}$, with E in GeV. It is the same, as in the second half of the 1994 running period and worse, compared to the 1992–93 conditions, where it was found to be $\sim 10\%/\sqrt{E}$.

As mentioned above, the choice of the E_{min} cutoff is dictated by the requirement of minimizing the overall systematic error $\delta\mathcal{L}$. Very qualitatively (quantitative arguments will be given later in this section, while describing each topic one by one in detail):

- low E_{min} leads to smaller pile-up effect corrections, but implies larger uncertainties in the trigger efficiency and in σ_{BH} (due to various coherent effects [6, 7]);
- high E_{min} increases the precision of the absolute photon energy scale (being closer to the sensitive area around the e$^+$ beam energy, used in the fit procedure described below), but implies larger pile-up effect corrections.

As a result, $E_{min} = 10$ GeV was found to be the optimal value, while $E_{min} = 5$ GeV and $E_{min} = 20$ GeV were used for cross checks, since they lead to partially different systematic errors.

4.2 e^+gas background

The background to reaction (1) is shown in Fig.3 as shaded histograms. It was determined from the e^+ pilot bunch events re-weighted with the factor $R_e = I_e^{total}/I_e^{pilot}$, and statistically subtracted from the full distributions. The fraction of the background events reflects the vacuum quality in the beam pipe around the IP. The long term history of the background conditions is shown in Fig.4.

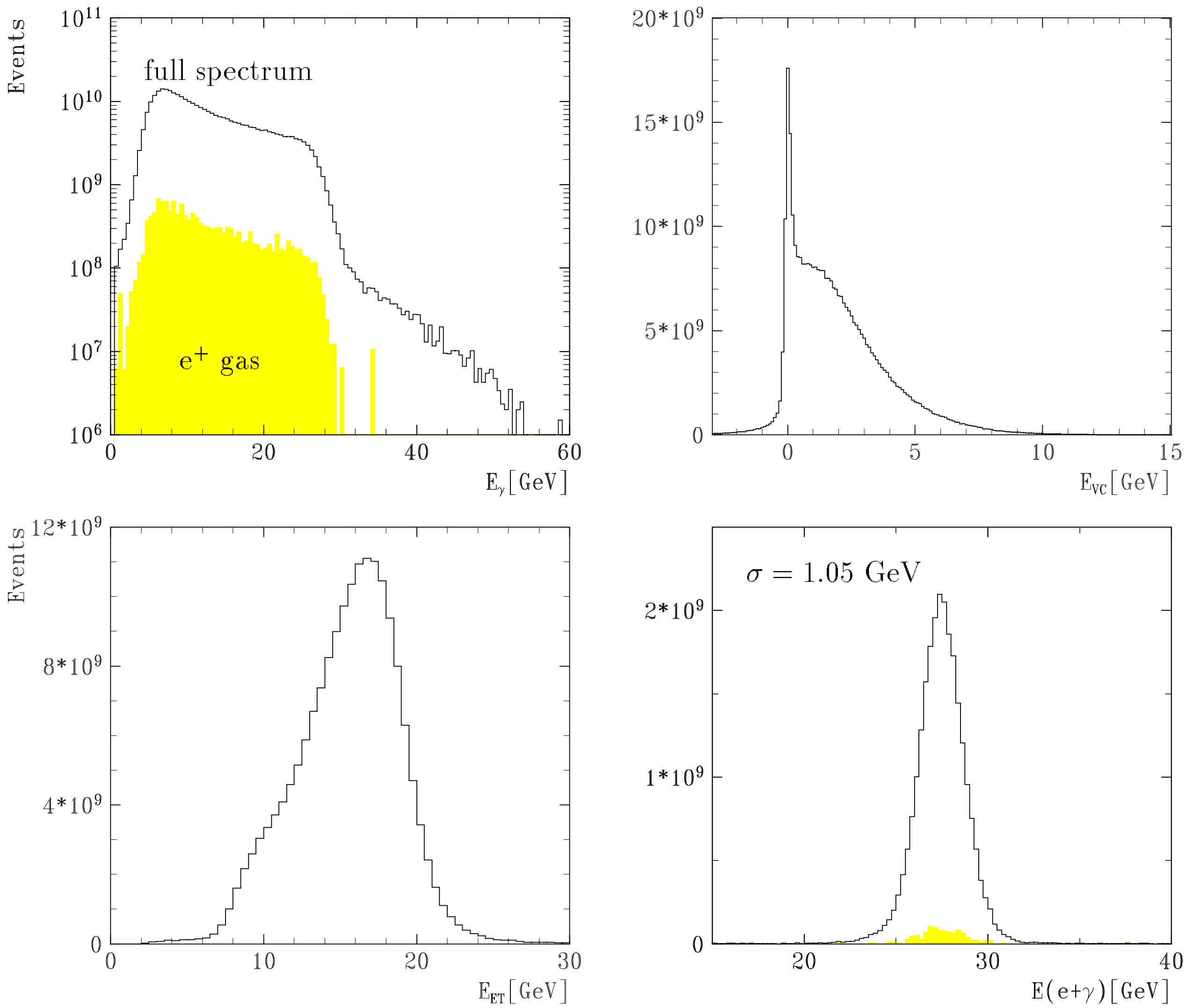

Figure 3: The energy spectra in the H1 Luminosity detectors for BH events triggered by the **s91** condition. Shaded histograms represent the background contribution.

One can see, that – as expected – the vacuum was improving significantly with time. Two exceptions in this plot are related to the accident with the vacuum leak (July-95) and to severe background conditions during the exercise with $z_{IP} = -70$ cm (November-95). A stable vacuum was achieved by the end of September-95, with a plateau level of about 2 times better than for the corresponding 1994 conditions, where it was $\sim 6-7\%$.

The average levels of the e^+gas bremsstrahlung background to reaction (1) in the three analyzed samples were as low as 4.4%, 3.9% and 8.2% respectively, thus enabling a high precision of the background subtraction to be reached.

It is interesting to look for a signal, originating from the positron annihilation on the electrons of the rest gas:

$$e^+e^- \rightarrow \gamma\gamma.$$

Such a process should lead to a visible "peak" in the E_γ distribution around the E_{e-beam}

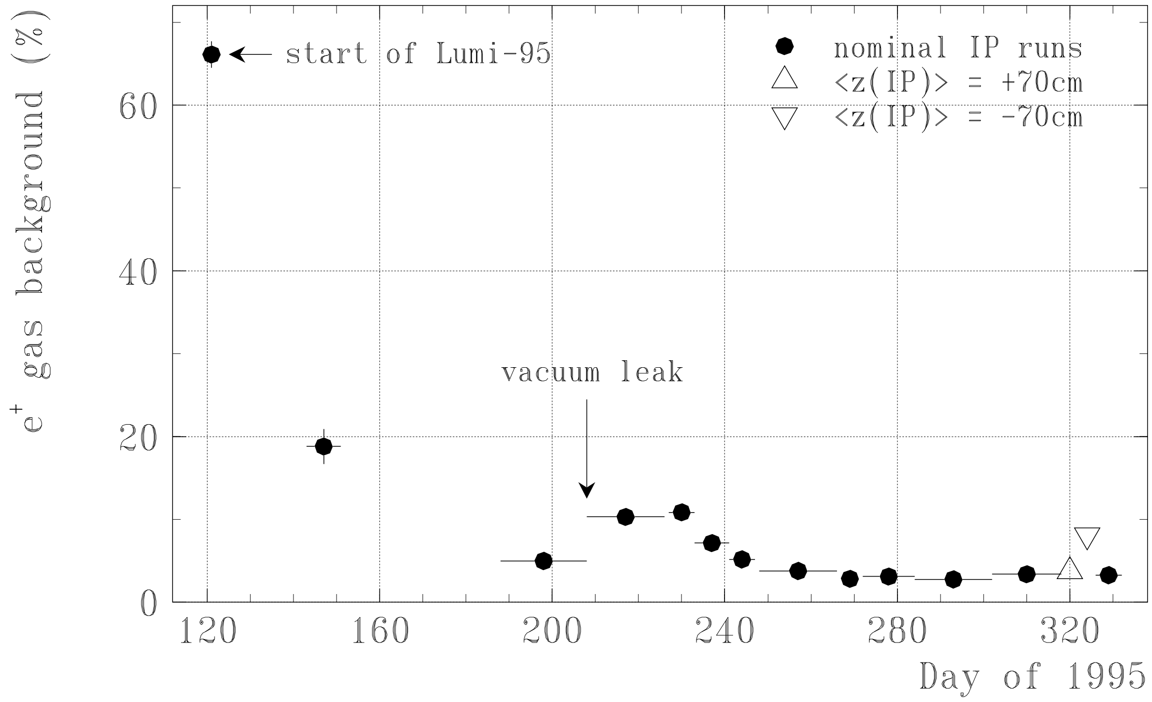

Figure 4: A long term history of the fraction of BH events, originating from e^+ gas bremsstrahlung.

energy. It can potentially be used as an additional method for the energy calibration of the photon arm. No significant deviation has been observed from the expected e^+ gas bremsstrahlung energy distribution, as illustrated by Fig.5. The comparison with the e^- gas data (from 1994 e^-p runs) leads to the same conclusion. The most obvious explanation of the absence of an e^+e^- annihilation contribution is that the residual gas in the beam pipe is highly ionized.

4.3 Trigger efficiency

The efficiencies of the trigger signals of the H1 Luminosity system are shown in Fig.6. The photon arm trigger efficiencies have been determined from the random trigger sample, while for the electron arm triggers the **s91** events were used.

One fact to notice is the "sharpness" of the PD trigger thresholds, which are visible better as a function of the deposited energy in the PD, compared to the total photon energy E_γ. The main reason is the influence of the Veto counter energy E_{VC}, which has large fluctuations. Another interesting point is the shape of the VC trigger efficiency curve as a function of the total photon energy. The plateau level is changing from ~0.8 to ~1.0 at high E_γ, reflecting the pile-up effect (multiple photons in the same bunch crossing). Note also that this plot represents in fact a convolution of the VC efficiency with the

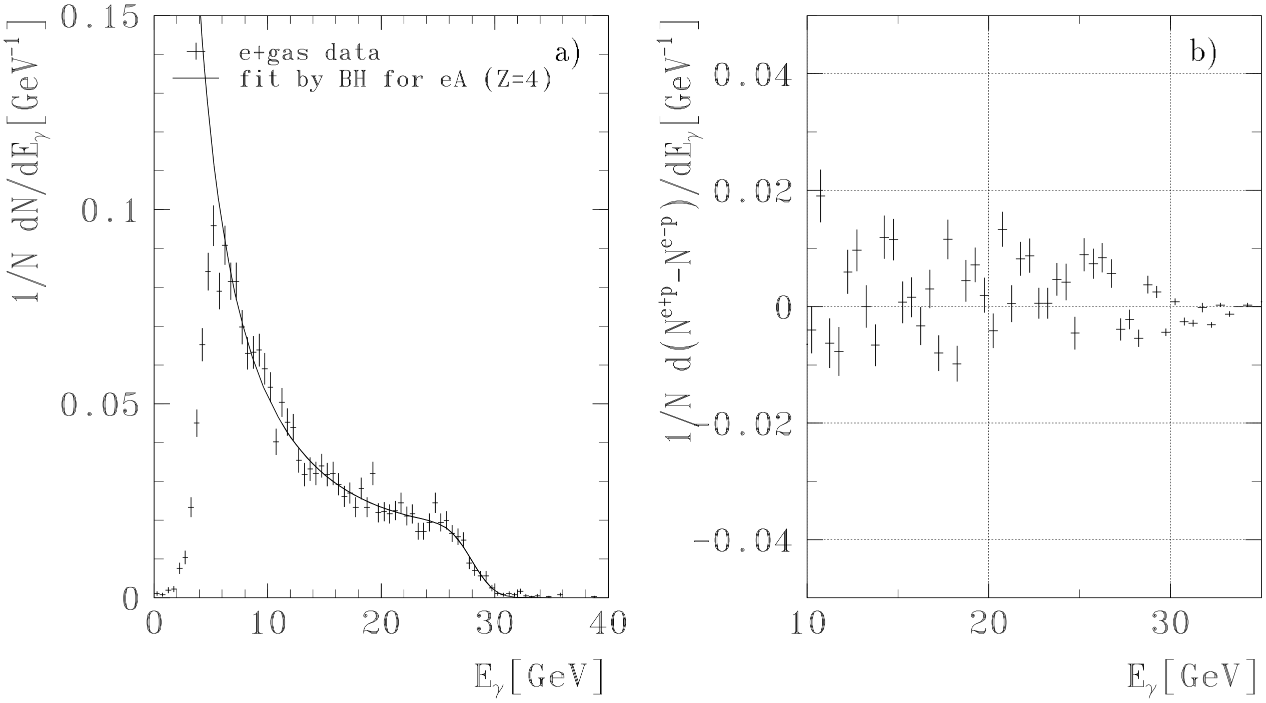

Figure 5: a) Photon energy distribution in e^+ pilot bunch events, compared to the BH cross section expectation for eA bremsstrahlung on $\overline{Z} = 4$ gas, taking into account the photon arm energy resolution; b) The difference between the normalized photon energy spectra, derived from the pilot bunch events of years 1995 (e^+ gas) and 1994 (e^- gas).

probability of the photon to convert within $3X_0$ material.

Most relevant for the present analysis is the efficiency of the subtrigger **s91**:

$$\epsilon_{s91}(E_\gamma > 10 \text{ GeV}) = 0.9977 \pm 0.0008.$$

4.4 Acceptance of the Photon Detector

The geometrical acceptance of the Photon detector for BH events is one of the most significant sources of systematic error in the luminosity measurement. It is mainly determined by the e^+ beam parameters, such as the horizontal and the vertical tilts θ_x, θ_y and the beam emittance, defining the angular divergence of the beam leptons and hence the radiated photons. The angular acceptance of the photon arm of the H1 Luminosity system is ~ 0.45 mrad, which is large compared to the typical "physics" angles of BH photons (~ 0.02 mrad). The angular divergences have to a good precision Gaussian shapes with the widths (at nominal e^+ beam optics [8]) $\sigma(\theta_x) \simeq 0.13$ mrad and $\sigma(\theta_y) \simeq 0.045$ mrad.

The beam tilt and divergence can be monitored experimentally by the coordinate distributions of photons in the Photon detector, as shown in Fig.7. The data are compared

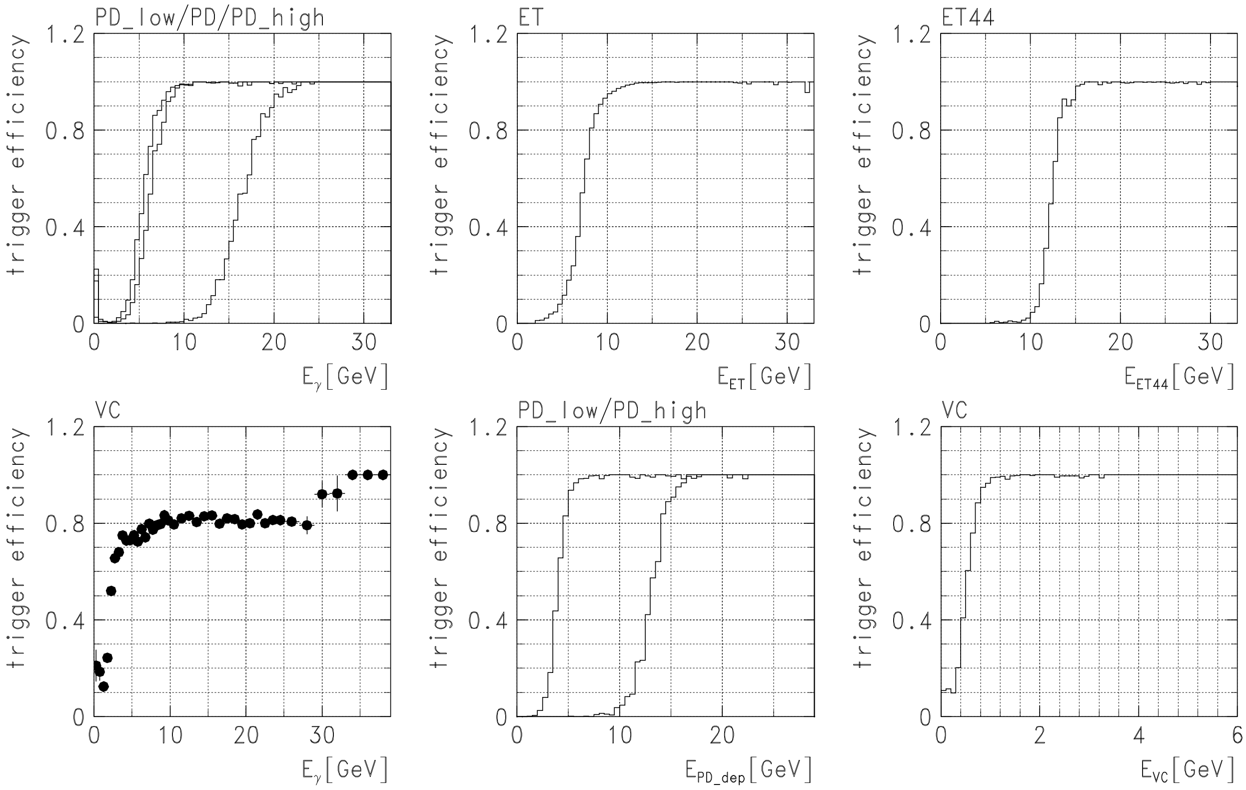

Figure 6: The trigger efficiencies of the Luminosity triggers in 1995.

to a Monte Carlo simulation [9], which takes into account real beam optics and the aperture limitations by the HERA magnet elements (clearly visible at the x-coordinate distribution tails).

The acceptance losses have been determined both from the Monte Carlo simulation using the lepton beam parameters, tuned to describe the measured coordinate distributions, and from the directly measured data by fitting the regions not affected by the aperture cuts. The main systematic error in this procedure is related to the short term variations of the beam tilt, caused by slight instabilities of the HERA magnets in the H1 IP region. Another source contributing to the systematic error is a possible deviation of the beam angular divergence distributions from the Gaussian shape (seen for example in the y-coordinate distribution). The final value for the photon detector acceptance, used in the integrated luminosity determination, is

$$< A_\gamma >= 0.972 \pm 0.006.$$

4.5 Photon Energy Scale

The determination of the absolute energy scale around the E_{min} cutoff is one of the most crucial problems of the offline luminosity determination.

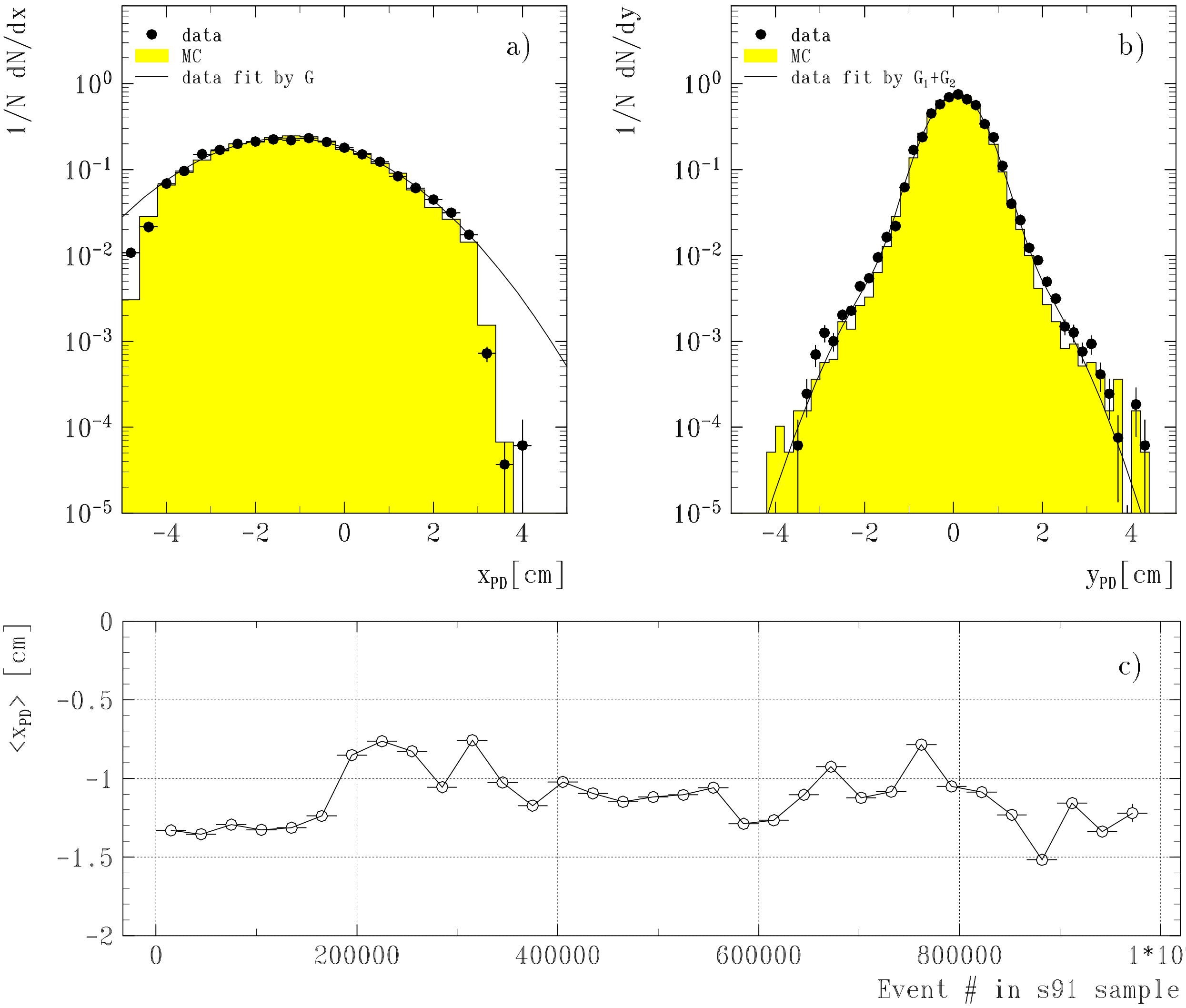

Figure 7: The photon coordinate distributions in PD (a,b) and the 1995 long term history of the horizontal position of the e$^+$ beam, $< x_{PD} >$ (c).

After an overall calibration of the system (using the constraint $E_e + E_\gamma = E_{e-beam}$), the photon energy scale is verified (and if necessary – corrected), by fitting the high energy part of the E_γ spectrum between (12±2) and (30±1) GeV to the BH formula [1], convoluted with the detector resolution function. The systematics of this method – including the energy scale shift due to the pile-up effect – have been studied with Monte Carlo simulated events. For the complete nominal IP sample the precision of the energy scale determination (at $E_\gamma \approx 25 - 30$ GeV) is

$$\delta E_{\gamma-scale}(27.5 \text{ GeV}) = 0.15\%.$$

To determine the absolute scale at smaller energies is more problematic. The linearity of the Photon detector itself has been studied in test beams in 1990–91, and was found to be better than 0.4%. However, the linearity of the whole photon arm, including the

Veto counter response, should be extracted from real data. One possibility is to exploit the energy correlation between the photon and the electron arms, as shown in Fig.8. Plotting the average value of $< E_e + E_\gamma >$ versus the photon energy, one can in principle

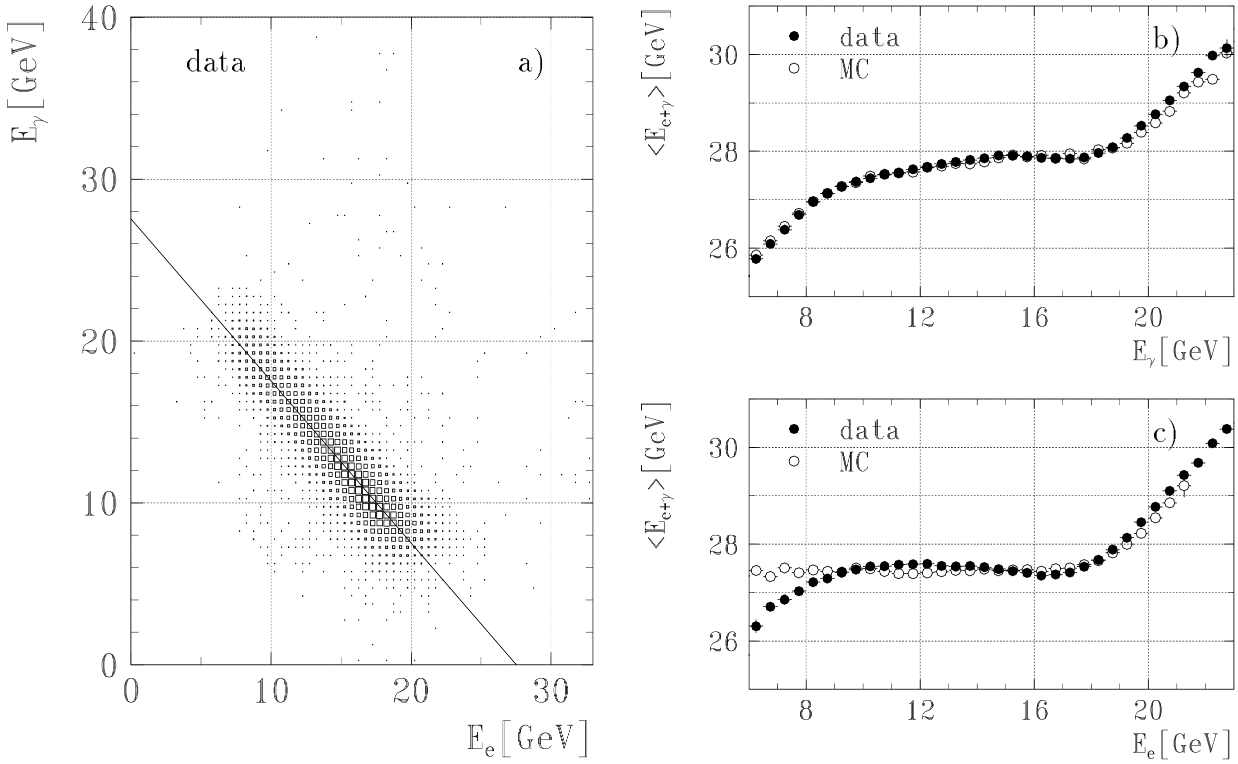

Figure 8: Energy correlations between the electron and the photon arms for BH events triggered by the coincidence requirement ET∗PD.

extract the information on the absolute scale at lower E_γ. Naively, any deviation from the constant level line in such a dependence would mean a nonlinearity of the energy scale. Unfortunately, this simple picture is not realised because of the limitations in the detector acceptances, especially the ET acceptance, which is strongly energy dependent. Therefore, it is necessary to compare the data with Monte Carlo events, having an ideal energy scale. Such a comparison is presented in Fig.8(b,c). For these plots the multiple photon events have been suppressed by the requirement $E_{VC} < 0.5$ GeV. One can see that the general trends are well reproduced by the Monte Carlo [9]. The residual differences, in the region of non-negligible ET acceptance, do not exceed 0.7%. They can be treated as a consequence of the non ideal Electron tagger acceptance description in the Monte Carlo. From that we conclude that the data are compatible with a simple scale error propagation:

$$\delta E_\gamma(E_{min}) = \delta E_\gamma(E_0) \frac{E_0}{E_{min}}.$$

The final step is to translate δE_γ to $\delta\mathcal{L}$ through the non-linear dependence $\delta\sigma_{BH}(\delta E_{min})$. As an example, the following systematic errors are obtained for the nominal IP data sample:

$$\delta\sigma_{BH} = \begin{cases} 0.74 \cdot \delta E_\gamma = 0.61\% & for\ E_{min} = \ 5\ GeV, \\ 1.13 \cdot \delta E_\gamma = 0.47\% & for\ E_{min} = 10\ GeV, \\ 2.98 \cdot \delta E_\gamma = 0.62\% & for\ E_{min} = 20\ GeV. \end{cases}$$

4.6 Pile-up Effect

The photon pile-up – i.e. more than one BH photon in the same bunch crossing and within the acceptance of the H1 Luminosity system – cannot be neglected at HERA. The probability P of the multiple photons ($n\gamma$) overlap is described by a Poisson distribution with mean value μ related to luminosity L,

$$\mu = \frac{\sigma_{BH}(E_\gamma > \epsilon) \cdot L}{f_{HERA} \cdot N_{ep}}, \tag{4}$$

where $\epsilon \approx 150$ MeV is the minimal energy at which photons can still penetrate the filter in front of VC and PD and deposit some visible energy response. N_{ep} is the number of colliding bunch pairs, and $f_{HERA} = 47.35$ kHz is the revolution frequency of the HERA machine. For $\mu \ll 1$, which is valid for all 1995 conditions ($N_{ep} = 174$), this leads to the simple relation

$$P(n\gamma) = 1 - e^{-\mu} \approx \ (3.2 \pm 0.2)\% \cdot L \tag{5}$$

with L in $\mu\mathrm{b}^{-1}\mathrm{s}^{-1}$. Main uncertainties come from the large corrections to the BH formula at such small energies [6, 7], and from the precision estimate of ϵ obtained in a detailed MC simulation of the photon arm response to low energy photons.

The photon pile-up leads to the following effects, which have to be corrected for:

1. the luminosity dependent shift of the energy scale in the fitting procedure of the E_γ spectrum and
2. the difference between visible and predicted (by σ_{BH}) number of photons with $E_\gamma > E_{min}$. The latter can in turn be further split into two parts:
   - the migration correction in $n\gamma$ events $C_{n\gamma}(E) = N^{true}_{BH}(E_\gamma > E)/N^{obs}_{BH}(E_\gamma > E)$,
   - the fraction of the $n\gamma$ events in the studied sample, which also depends on the value of E_{min}.

   Thus, the final $\delta_{n\gamma}$ correction factor in (3) depends both on L and E_{min}.

Note, that in practice we only account for up to 3γ overlaps, neglecting 4 and more photon events, as their probability is very small at present HERA luminosities.

The pile-up effect has been studied using a large statistics H1LUMI MC simulation [9] with the real energy resolution as derived from data. The results are summarized in Fig.9. As seen, $E_{min} = 5$ GeV is the best value for minimizing the pile-up corrections. In fact, at this value the migrations are fully compensated. The luminosity dependence of the

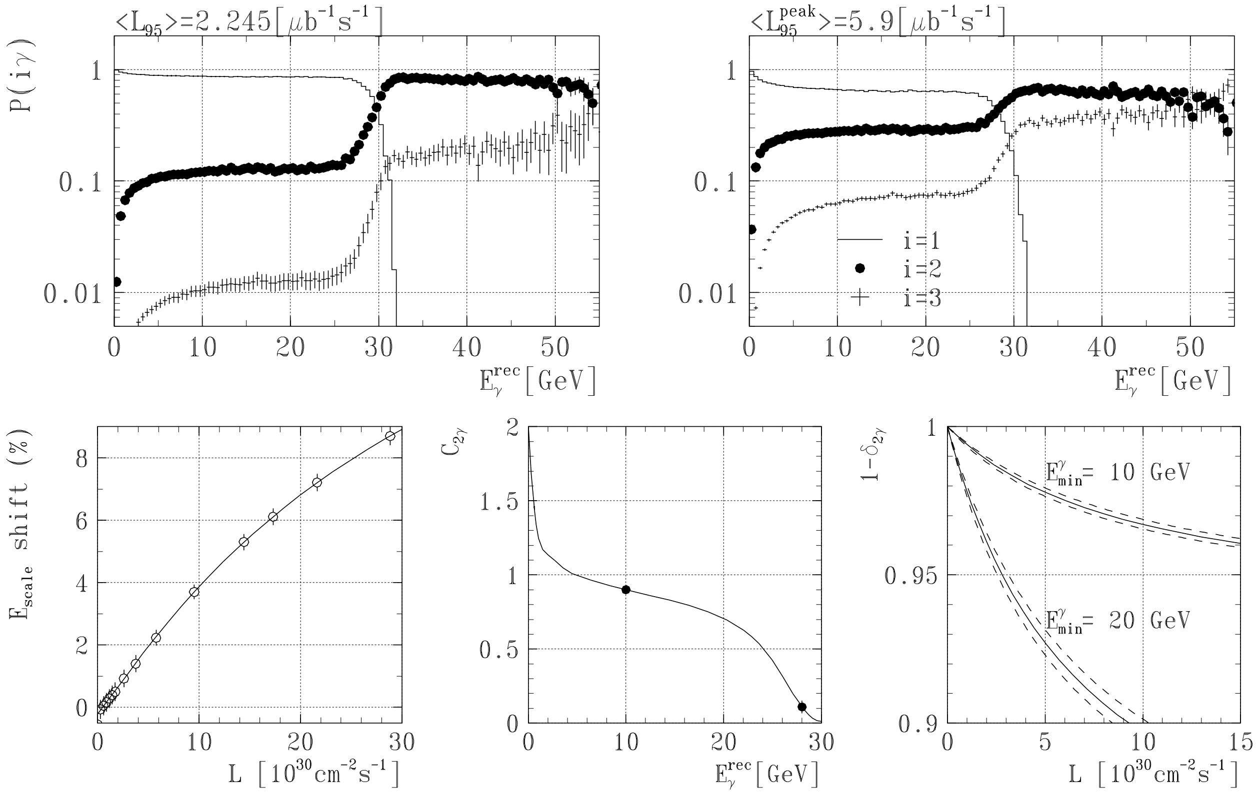

Figure 9: MC simulation of the photon pile-up effect. Top: relative fractions of the events with different photon multiplicities. Bottom: correction factors used for the offline $\mathcal{L}_{1995}$ determination. Symbols and dashed curves represent the systematic errors of the corresponding factors. E_{scale} refers to the PD energy calibration.

2γ overlap correction factor for the two other values of E_{min} is shown in the last plot of Fig.9. The dashed curves correspond to the systematic error band.

Fig. 10 shows the photon energy distributions in the three data samples of 1995, compared to Monte Carlo expectations taking into account 2γ and 3γ overlap events. The agreement between the data and Monte Carlo at $E_\gamma \geq 10$ GeV is good. The discrepancy at smaller energies is due to the trigger threshold, which is not simulated in this study.

4.7 Corrections to the Online Luminosity

The final result for the luminosity, obtained with $E_{min} = 10$ GeV, is presented in Fig.11 as corrections to the online luminosity measurements for the 19 different run ranges of 1995. The correction is defined as $\Delta\mathcal{L} = (\mathcal{L}_{offline} - \mathcal{L}_{online})/\mathcal{L}_{online}$.

There is an obvious correlation between the size of the luminosity correction and the horizontal offset of the e beam in the interaction region, as measured by the central tracking chambers [10]. It is known, that the ET acceptance is very sensitive to both the beam tilt and the beam position in the horizontal direction. Thus, the result shown in Fig.11 confirms the hypothesis that the Electron tagger acceptance variation is the main reason for the systematic error in the absolute luminosity determination by the coincidence method.

On average, the corrections to the online integrated luminosity for the three main data samples are:

Data sample	Nominal IP	$< z(IP) >= +70$cm	$< z(IP) >= -70$cm
$\Delta\mathcal{L}$	-2.7%	-5.4%	-1.2%

A cross check has been performed for the nominal IP sample by using $E_{min} = 5$ GeV and $E_{min} = 20$ GeV. The result, presented in Table 5, shows no apparent problems in the analysis. Note, that the common part of the systematic error is excluded from the table and from the comparison of the three $\mathcal{L}$ values obtained.

Value	Unit	$E_{min} = 5$ GeV	$E_{min} = 10$ GeV	$E_{min} = 20$ GeV
$\sum W_{ep}$	$[10^9]$	298.41 ± 0.48	180.46 ± 0.38	54.28 ± 0.20
ϵ_{s91}		0.9035 ± 0.0031	0.9977 ± 0.0008	0.9989 ± 0.0006
$\delta_{n\gamma}$		0.0	0.0123 ± 0.0011	0.0425 ± 0.0036
σ_{BH}^{acc}	[mb]	69.31 ± 0.50	37.28 ± 0.18	10.83 ± 0.07
$\mathcal{L}$	$[\mathrm{nb}^{-1}]$	4765 ± 38	4792 ± 24	4805 ± 38
$R = \frac{\mathcal{L}(E_{min})}{\mathcal{L}(E_{min}=10GeV)}$		0.9944 ± 0.0094	1.0	1.0027 ± 0.0094

Table 5: Comparison of the integrated luminosity values for the nominal IP sample, obtained by using different E_{min} cutoffs. The common part of the systematic error is excluded from the table. σ_{BH}^{acc} is the acceptance corrected BH cross section.

4.8 Systematic Error Summary

All contributions to the overall systematic error $\delta\mathcal{L}$ are collected in Table 6. For comparison, the precisions of the integrated luminosity determination in previous years are included as well. Some of the systematic error contributions for 1994 data were re-evaluated in order to be consistent with the present analysis (i.e. to have the same meaning). It is very hard to improve further the precision of the luminosity measurement in this method.

The "Rounding errors" row refers to the precision of calculating the integrated run luminosity, including corrections for the detector HV status. This is in general analysis dependent, because different physics analyses require different H1 configurations.

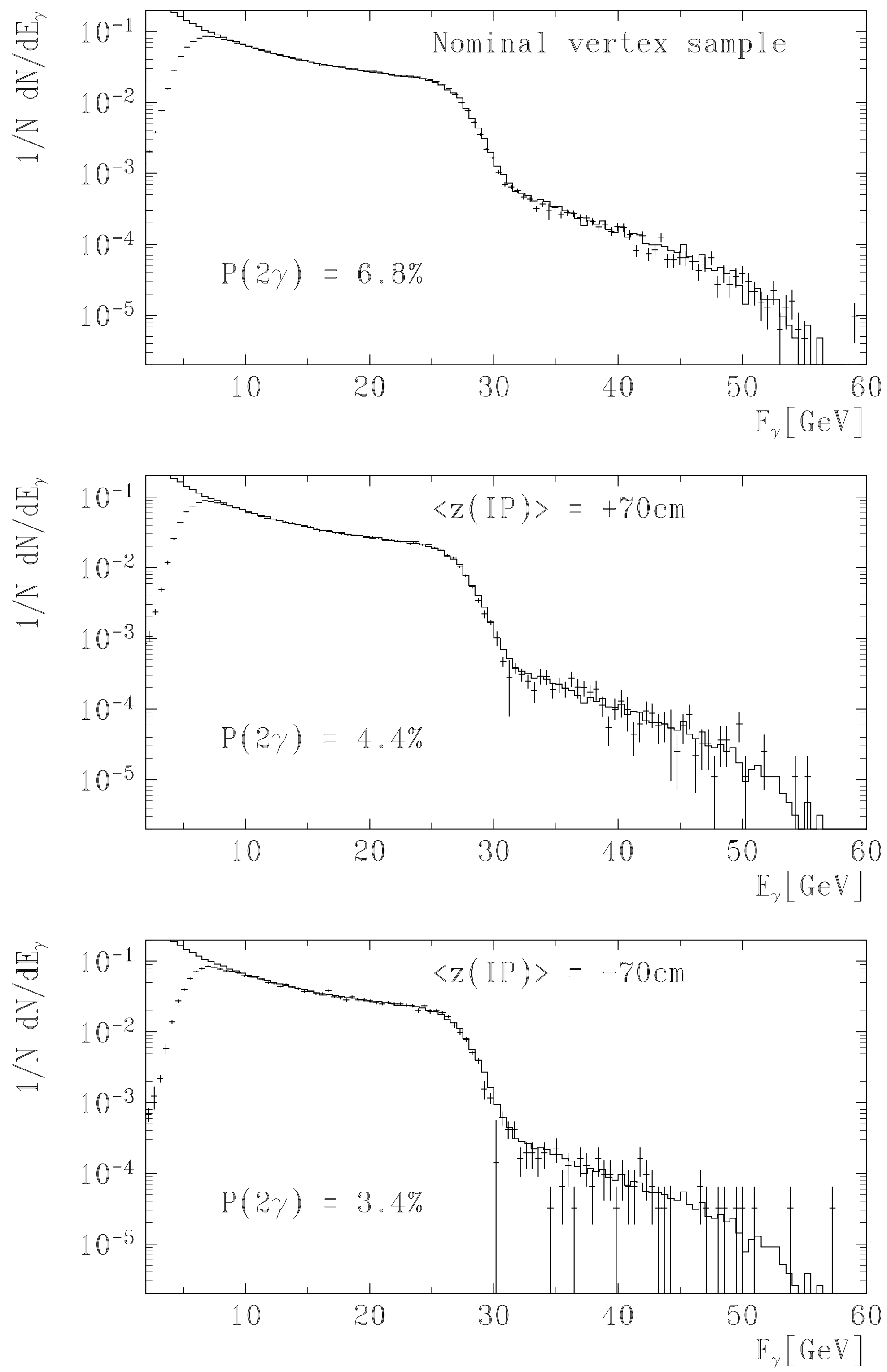

Figure 10: The photon energy spectra (symbols) in the three different data samples of 1995, compared to Monte Carlo expectations (histograms) taking into account the detector resolution and the multiple photon overlap effects. The probabilities $P(n\gamma)$ used in the MC simulation were calculated using eqs.(4, 5) and actual integrated luminosities, averaged over all runs in a given sample.

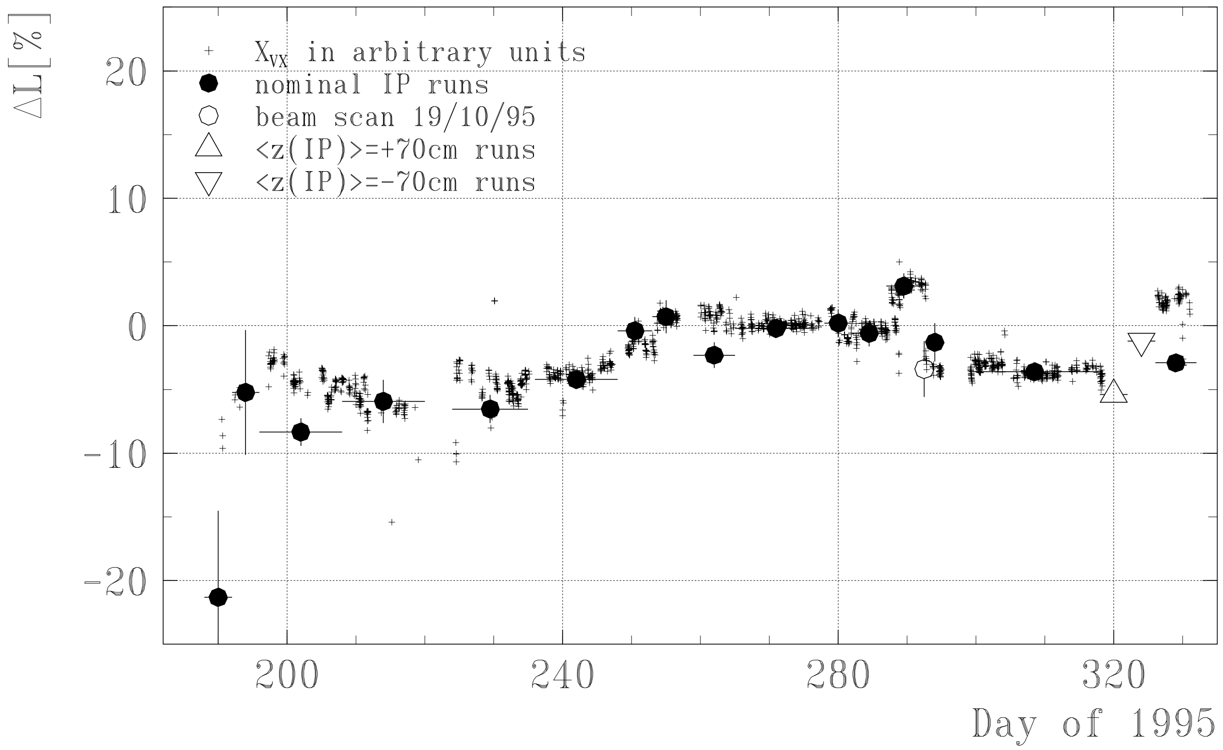

Figure 11: Offline corrections to the 1995 online luminosity measurements. Overlayed (as small crosses) are the horizontal positions of the e^+p event vertices (in arbitrary units) as measured by the central tracking chamber.

Contribution to $\delta\mathcal{L}$	1993	1994			1995		
		e^-p	e^+p	+70cm	nominal	+70cm	−70cm
1. Theoretical value for σ_{BH}	0.5		0.5			0.5	
2. Trigger efficiency	2.0		0.3			0.1	
3. Statistics, e-gas bgr. subtraction	1.5	1.3	0.4	3.3	0.21	0.41	0.77
4. γ-energy scale (calib. & resol.)	1.7	1.2	1.0	1.7	0.47	0.50	0.79
5. Geometrical acceptance of γ-arm	0.7		0.5			0.6	
6. Multiple photon effect (pile-up)	0.2		0.1		0.11	0.09	0.06
7. Rounding errors (HV corr. etc.)	1.1		0.5			0.5	
Total error from the Lumi system	3.4	2.0	1.4	3.8	1.07	1.14	1.45

Table 6: Precision (in %) of the H1 integrated luminosity determination in 1995, compared to 1993 and 1994 data.

5 Conclusions

The final results are summarized in Table 7. We conclude that high precision is achieved in the determination of the integrated luminosity for the 1995 data samples.

Room for possible improvements is related to the theoretical precision of the BH cross section calculation, used for normalization. The numerical evaluation of higher order corrections and various coherent effects is necessary to reach the ultimate precision in this area.

Data sample	nominal IP	$< z(IP) >= +70$cm	$< z(IP) >= -70$cm
$\Delta\mathcal{L}_{\text{off}}(\%)$	-2.7	-5.4	-1.2
$\delta\mathcal{L}_{\text{lumi}}(\%)$	1.07	1.14	1.45

Table 7: Average corrections $\Delta\mathcal{L}_{\text{off}}$ to the online luminosity measurement for the 1995 data samples, and precision $\delta\mathcal{L}_{\text{lumi}}$ of the integrated luminosity determination.

Acknowledgements

We are grateful to the HERA machine group whose outstanding efforts have made and continue to make this experiment possible. We thank the engineers and technicians for their work in constructing and now maintaining the H1 detector, our funding agencies for financial support, the DESY technical staff for continual assistance, and the DESY directorate for the hospitality which they extend to the non–DESY members of the collaboration.

References

[1] H.Bethe and W.Heitler, Proc. Roy. Soc. **A146** (1934) 83.

[2] H1 Collaboration (T. Ahmed et al.), Experimental Study of Hard Photon Radiation Processes at HERA. Z.Phys. C66 (1995) 529-542.

[3] N.Gogitidze, H1 LUMI System Status Report. H1 Collaboration meeting, DESY, Hamburg, Germany, 13-Oct-1994.

[4] FEU - 147, MELZ, Moscow, Russia.

[5] Creative Electronics Systems SA, Fast intelligent controller FIC 8230/8232. Geneva, CH (1987/1992).

[6] G.L.Kotkin, S.I.Polityko, A.Schiller and V.G.Serbo, Z.Phys. **C39** (1988) 61.

[7] K.Piotrzkowski, Z.Phys. **C67** (1995) 577.

[8] G.Wolf, HERA: Physics, Machine and Experiments, DESY 86-089 (1986).

[9] S.Levonian, H1LUMI - A Fast Simulation Package for the H1 Luminosity System, H1 note H1-04/93-287 (1993).

[10] V.Blobel and L.Criegee, ONLINE monitoring and determination of run-dependent calibration constants within reconstruction modules, H1 s/w note 41 (1993).